Check for updates

Integrated perovskite solar capacitors with high energy conversion efficiency and fast photo-charging rate†

Jia Liang,‡[a] Guoyin Zhu,‡[a] Zhipeng Lu,[a] Peiyang Zhao,[a] Caixing Wang,[a] Yue Ma,[a] Zhaoran Xu,[a] Yanrong Wang,[a] Yi Hu,[a] Lianbo Ma, [ID][a] Tao Chen,[a] Zuoxiu Tie,[a] Jie Liu[ab] and Zhong Jin [ID] *[a]

Integrating energy harvesting devices with energy storage systems can realize a temporal buffer for local power generation and power consumption. In this manner, self-charging energy devices consisting of photovoltaic cells and energy storage units can serve as sustainable and portable distributed power sources that can concurrently generate and store electric energy without the need for external charging circuits. Herein, an integrated perovskite solar capacitor (IPSC) was realized by combining a perovskite solar cell (PSC) and a supercapacitor in a single device. Taking advantages of nanocarbon electrodes, the IPSCs possess a simple configuration, compact structure, and well-matched operation voltage. The IPSCs could be rapidly charged by different modes (including the photo-charging mode, galvanostatic-charging mode, and photoassisted-galvanostatic-charging mode), and showed a remarkable overall photo-chemical-electricity energy conversion efficiency as high as 7.1% in the photo-charging mode. Moreover, the IPSCs could work efficiently under weak light illumination. This study provides new insights for the design of novel integrative energy devices that combine the functions of solar power harvesting and electrochemical energy storage.

Introduction

With the rapidly increasing global demands for green energy, the research on portable power supplies and integrated energy devices are making steady progress.[1-3] Among the renewable energy sources, solar power holds great promise owing to its high abundance, easy accessibility, local applicability, and cleanliness.[4-8] In recent years, hybrid organic–inorganic metal halide perovskites have emerged as promising candidates for efficient solar energy harvesting, owing to their exceptional optoelectronic properties, such as tunable band gap, large absorption coefficient, high charge carrier mobility, and long electron–hole diffusion distance.[9-13] Based on these merits, perovskite solar cells (PSCs) have attracted tremendous attention over the past few years.[14-24] The power conversion efficiency (PCE) of PSCs has exhibited a meteoric rise and reached up to 22.1%, and have shown the potential to approach the Shockley–Queisser limit of a single-junction solar cell.[25] To promote the

[a]Key Laboratory of Mesoscopic Chemistry of MOE, School of Chemistry and Chemical Engineering, Nanjing University, Nanjing, Jiangsu 210023, China. E-mail: zhongjin@nju.edu.cn

[b]Department of Chemistry, Duke University, Durham, NC 27708, USA

† Electronic supplementary information (ESI) available. See DOI: 10.1039/c7ta09099d

‡ These authors contributed equally to this work.

practical application of PSCs, it is essential to develop large-area, low-cost, scalable, and printable PSCs. In the aspect of counter electrode materials, nanocarbons are considered as promising candidates to replace expensive noble metal electrodes, bring the advantages of high conductivity, excellent stability, easy processability, low cost, and good compatibility to printing technology.[17,26-33]

Nevertheless, it should be noted that while solar cells can generate power under the sun, they cannot store energy. The power output of solar cells is restricted by the ambient factors, such as the light intensity, temperature, weather, location, and day–night cycle, thus their deployment as ready-to-use portable power supplies is seriously limited. To alleviate this problem, considerable attempts have been made to develop novel integrated energy systems that combine the functions of both photovoltaic cells and energy storage units into a single device.[1-3,34-50] These integrated "photo-charging" energy systems can simultaneously achieve photoelectric conversion and electrochemical energy storage, so that they can provide a stable and continuous source of power output that avoids the fluctuations induced by the change in transient daylight intensity and the diurnal cycle. However, due to the low open voltages of photovoltaic cells, the operating voltage of the present integrated photo-charging energy systems are relatively low (usually 0.5–0.7 V), and the overall energy conversion efficiencies are still not very satisfying (normally 0.8–4.7%), as summarized in

This journal is © The Royal Society of Chemistry 2018

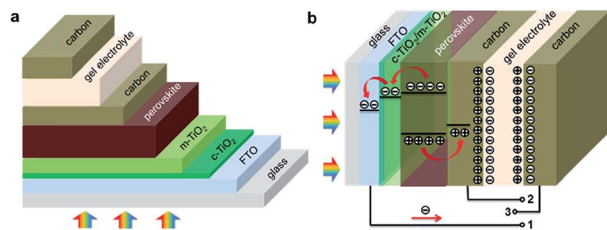*J. Mater. Chem. A*, 2018, **6**, 2047–2052 | **2047**

Fig. 1 (a) Schematic configuration and (b) operating mechanism of the IPSC realized by combining a PSC and a supercapacitor into a single device.

Table S1.† To simultaneously realize a high overall efficiency, reasonable energy density, fast charging rate, and long cycling life, the device architecture and material compositions of self-powering energy systems need careful design and construction.

For the construction of integrated photo-charging energy devices, supercapacitors can serve as a good option for energy storage units, and benefit from an ultrahigh power density, excellent cycling stability, and good safety.[51–60] Besides, the operation voltage of supercapacitors matches very well with the output voltage of solar cells. Notably, the state-of-the art electrode materials of supercapacitors are generally nanoporous carbons or carbon-based composites.[51–58] Therefore, nanocarbons can simultaneously serve as both the counter electrode of PSCs[13,23–30] and as the electrode materials of supercapacitors, thus can play an important role in integrated photo-charging energy devices.

Following this line of thought, here we report an integrated perovskite solar capacitor (IPSC) constructed by combining the units of a perovskite solar cell and a solid-state supercapacitor together, for the in-sync realization of photovoltaic conversion and electrochemical energy storage (Fig. 1). Benefiting from nanocarbon electrodes, the IPSC had a compact architecture and well-stacked interfaces for the process of charge generation, transfer, and storage. The IPSC showed a high operation voltage (0.91 V) and a high overall photo-chemical-electricity energy conversion efficiency of 7.1%. Remarkably, the IPSC could work efficiently under weak light environment and could be photo-charged at any stage of the charging/discharging process.

Experimental

Fabrication of IPSC

FTO conductive glass (with the FTO thickness of ∼1 μm) was first etched by 2.0 M HCl solution and Zn powder to obtain the desired patterns. Then the FTO glass was sequentially ultra-sonically cleaned with acetone, ethanol, and deionized water. The c-TiO_2 layer was deposited on the FTO substrate by spin-coating an ethanol solution of titanium isopropoxide (0.5 M) and diethanol amine (0.5 M) at 7000 rpm for 30 s, and then the substrate was annealed at 500 °C for 2 h in air. The m-TiO_2 layer was then deposited by spin-coating a mixture of TiO_2 paste and ethanol 1 : 8 (w/w) at 5000 rpm for 30 s, and then sintered at 500 °C for 30 min in air. Then, the FTO substrate was immersed in a $TiCl_4$ solution of 40 mM at 70 °C for 30 min, cleaned with

water and ethanol, and then annealed at 450 °C for another 30 min.

Subsequently, the $MAPbI_3$ layer was introduced using a two-step deposition method in an Ar-filled glovebox. Typically, a 1.0 M dimethylformamide (DMF) solution of PbI_2 was spin-coated on the substrate at 3000 rpm for 30 s, and then dried at 70 °C for 30 min. Then, the substrate was dipped in an isopropoxide solution of 10 mg mL^{-1} MAI for 120 s, washed with isopropoxide, dried by N_2 gas, and then annealed at 100 °C for 10 min. The carbon layer serving as both the hole-transfer layer and the counter electrode of PSC (#2) was deposited by the doctor-blade coating of commercially-available conductive carbon ink on the $MAPbI_3$ layer using adhesive tapes as the spacer, and then heated at 70 °C for 60 min.

The gel electrolyte layer for the supercapacitor unit was prepared by dissolving 3.0 g concentrated H_3PO_4 and 3.0 g PVA in 30 mL deionized water. The mixture was heated at 85 °C under vigorous stirring until the solution became clear. The viscous gel electrolyte was carefully deposited on the carbon layer and heated at 70 °C for 2 min. Finally, another carbon layer serving as the anode of the supercapacitor unit (#3) was deposited on the gel electrolyte layer following the above-mentioned doctor-blade coating method.

Characterizations

The morphological features of the samples were examined by field-emission SEM (HITACH S-4800). The crystal structures of the samples were analyzed by XRD with a Bruker D-8 Advance Diffractometer using Cu Kα X-ray radiation. The light absorbance spectra were collected with a UV-vis-NIR spectrophotometer (Shimadzu, UV-2800). The PL emission spectra were recorded on a home-built wide-field fluorescence microscope under an excitation wavelength of 532 nm.

Measurements of IPSC

The photovoltaic performances of the PSC unit in IPSC were measured under simulated AM1.5G solar illumination provided by a solar simulator (Oriel Solar Simulator, Model 91160, AAA class). The current–voltage characteristics were recorded by a Keithley 2400 source meter. The photocurrent density–voltage (J–V) curves of the PSC unit were measured at a scan rate of 100 mV s^{-1}.

The CV and galvanostatic-charging/galvanostatic-discharging characteristics of the supercapacitor unit in the IPSC were evaluated by a Chenhua CHI-760E electrochemical workstation. The CV curves were measured by sweeping the voltage from 0–1.0 V at different scan rates. The galvanostatic-charging/galvanostatic-discharging curves were recorded between 0–1.0 V at different current densities. The areal specific capacitance (C_a), areal energy density (E_a), and areal power density (P_a) of the supercapacitor unit were calculated by using the following equations:

$$C_a = I\Delta t/A\Delta V$$

$$E_a = C_a\Delta V^2/7200$$

2048 | J. Mater. Chem. A, 2018, **6**, 2047–2052

This journal is © The Royal Society of Chemistry 2018

$$P_a = E_a \times 3600/\Delta t = C_a \Delta V^2/2\Delta t$$

where I is the current, Δt is the discharge time, ΔV is the potential window, and A is the effective area of the electrode.

The photo-charging/galvanostatic-discharging curves of the IPSC were measured. First, the IPSC was photo-charged under simulated solar illumination with the designated light intensities to reach the voltage plateau (0.91 V). Then, the light was turned off and the IPSC was galvanostatic-discharged at the designated current densities.

The photoassisted-galvanostatic-charging/galvanostatic-discharging mode of IPSC was also tested. The IPSC was first charged to 0.91 V by galvanostatic-charging coupled with different durations of photo-charging, then the light was shut off and the IPSC was further charged to 1.0 V by still-ongoing galvanostatic-charging. Then, the IPSC was galvanostatic-discharged to 0 V at the designated current densities.

Results and discussion

Fig. 1a shows the schematics view of the IPSC combining a PSC and a supercapacitor with functional layers of fluorine-doped tin oxide (FTO)/compact-TiO$_2$ (c-TiO$_2$)/mesoporous-TiO$_2$ (m-TiO$_2$)/MAPbI$_3$ (MA = CH$_3$NH$_3^+$)/carbon/gel electrolyte/ carbon. The working mechanism of IPSC is displayed in Fig. 1b. The PSC unit acted as the photo-electricity conversion part, consisting of FTO/c-TiO$_2$/m-TiO$_2$/MAPbI$_3$/carbon layers. The supercapacitor unit contained carbon/gel electrolyte/ carbon layers. The carbon electrode (#2) between the MAPbI$_3$ and gel electrolyte layers served as both the counter electrode of PSC and the cathode of the supercapacitor. To achieve the photo-charging of the IPSC under illumination, the working electrode of the PSC unit (#1) and the anode of the super-capacitor unit (#3) were connected. During the photo-charging process, the MAPbI$_3$ layer absorbs light and generates electron–hole pairs. The electron–hole pairs are rapidly separated. The electrons are transferred to the anode of the supercapacitor unit (#3); meanwhile, the holes are stored by the shared carbon electrode of the PSC and supercapacitor (#2). In this way, continuous light illumination on the PSC unit can achieve efficient photo-charge generation and transfer, and thus can result in the fast charging of the supercapacitor unit. When the voltage between the cathode and anode of supercapacitor unit is close to the open voltage (V_{OC}) of the PSC unit, the photo-charging process temporarily stops. As a result, the solar power is converted into electric energy by the PSC unit, and then stored into the supercapacitor unit as electrochemical energy, which can be conveniently released again by galvanostatic-discharging, just like with conventional supercapacitors.

Fig. 2a and b display the cross-sectional scanning electron microscopy (SEM) images of the IPSC device and the magnified PSC unit, respectively, showing the uniformly-stacked FTO/c-TiO$_2$/m-TiO$_2$/MAPbI$_3$/carbon/gel electrolyte/carbon functional layers. The homogeneous surface features of the c-TiO$_2$ and m-TiO$_2$ layers are shown in Fig. S1a and b,† respectively. Fig. S2† exhibits the SEM image of the nanocarbon electrode in the IPSC, which consists of carbon nanoparticles with an average
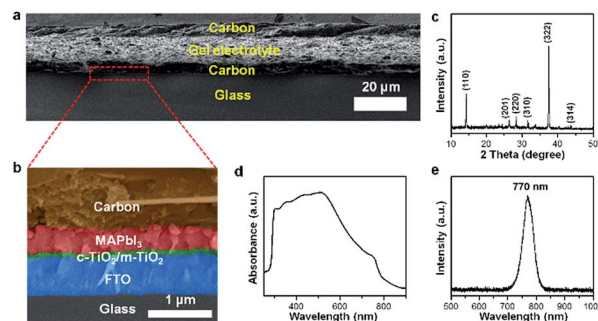

Fig. 2 (a) Cross-sectional SEM image of the IPSC with functional layers of FTO/c-TiO$_2$/m-TiO$_2$/MAPbI$_3$/carbon/gel electrolyte/carbon. (b) Cross-sectional SEM image (with pseudo-colors) of the magnified PSC unit in the IPSC of (a). (c) XRD pattern, (d) absorbance spectrum and (e) PL emission spectrum of the MAPbI$_3$ layer, respectively.

diameter of ~80 nm. The XRD pattern of the MAPbI$_3$ layer shows strong diffraction peaks corresponding to the (110), (201), (220), (310), (322), and (314) lattice planes of MAPbI$_3$ (Fig. 2c).[61] The UV-vis absorbance spectra of MAPbI$_3$ layer shows a light-absorption onset wavelength around 780 nm (Fig. 2d), and the peak position of the photoluminescence (PL) emission spectrum of MAPbI$_3$ layer is ~770 nm (Fig. 2e), whereby both indicate that the optical bandgap is about 1.6 eV.

The performances of the PSC unit in the IPSC were examined. Fig. 3a shows the photocurrent density–voltage (J–V) curves of the PSC unit under simulated AM1.5G solar light with different illumination intensities (45–100 mW cm^{-2}). The corresponding photovoltaic parameters, including the short-circuit density (J_{SC}), open-circuit voltage (V_{OC}), fill factor (FF), and power conversion efficiency (PCE), are summarized in Table S2.† At the light intensity of 100 mW cm^{-2}, the IPSC showed a PCE as high as 8.9% with a V_{OC} of 0.92 V, which is remarkable among the literature reports.[1–3,38–50] Under different light intensities, the values of V_{OC}, FF, and PCE showed minimal changes. At the light intensity of 45 mW cm^{-2}, the value of PCE increased to 9.6%, indicating the good performance under weak light illumination. The histogram of the PCE values of 40 individual IPSC devices at 100 mW cm^{-2} are shown in Fig. 3b, showing an average value of 8.2% and a narrow distribution, demonstrating the good reproducibility originating from the high quality and homogeneous thickness of the functional layers.

The electrochemical properties of the supercapacitor unit in the IPSC were also investigated. Fig. 3c shows the cyclic voltammetry (CV) curves of the supercapacitor unit at different scan rates (20–100 mV s^{-1}) in a voltage window of 0–1.0 V. The CV curves retain an approximately rectangular shape, indicating the high electrochemical performance of the supercapacitor unit during fast charge–discharge processes. The galvanostatic charge/discharge curves of the supercapacitor unit were measured at different current densities (0.1–0.5 mA cm^{-2}, Fig. 3d). At relatively high current densities, the galvanostatic charge/discharge curves have a relatively symmetric triangle shape, indicating the charge-storage behavior of electrical double-layers. According to the charge/discharge curves, the
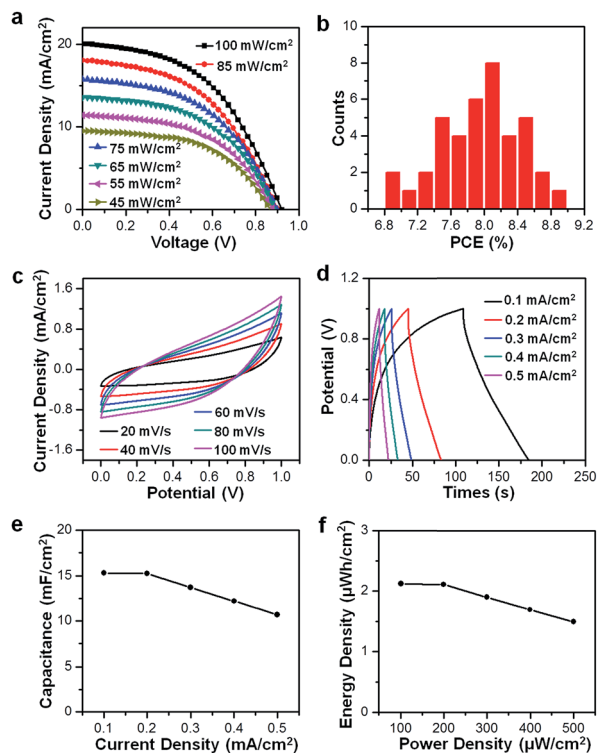
This journal is © The Royal Society of Chemistry 2018

J. Mater. Chem. A, 2018, 6, 2047–2052 | 2049

Fig. 3 (a) $J-V$ plots of the PSC unit in an IPSC under different simulated solar illumination intensities (45–100 mW cm^{-2}). (b) Statistical histogram of the PCEs of 40 individual IPSCs at the light intensity of 100 mW cm^{-2} (c) CV curves and (d) galvanostatic charge/discharge curves of the supercapacitor unit in an IPSC. (e) Capacitances and (f) Ragone plot of the supercapacitor unit in an IPSC at different current densities.

Fig. 4 (a) Photo-charging/galvanostatic-discharging curves of the IPSC under fixed simulated AM1.5G solar illumination intensity (100 mW cm^{-2} at charging stages) and different discharging current densities (0.2–0.5 mA cm^{-2} at discharging stages). The period of light illumination is highlighted by the light-red color. (b) Photo-charging/galvanostatic-discharging curves of the IPSC under different simulated solar illumination intensities (45–100 mW cm^{-2} at charging stages) and a fixed discharging current density (0.4 mA cm^{-2} at discharging stages). (c) Photo-charging/galvanostatic-discharging curves of the IPSC with different intervals of simulated solar illumination (100 mW cm^{-2}) and fixed discharging current density (0.4 mA cm^{-2} at discharging stages). (d) Photoassisted-galvanostatic-charging/galvanostatic-discharging curves of the IPSC with different durations of simulated solar illumination (100 mW cm^{-2} at charging stages) and a fixed discharging current density (0.4 mA cm^{-2} at both charging and discharging stages). (e) $\eta-t$ curves of the IPSC under different simulated solar illumination intensities (45–100 mW cm^{-2}).

charge-storage capacitances of the supercapacitor unit at different current densities were calculated (Fig. 3e). As the current density increased from 0.1 to 0.5 mA cm^{-2}, the areal capacitance changed from 15.3 mF cm^{-2} to 10.7 mF cm^{-2}, suggesting the good rate capability. To evaluate the correlation between the power density and energy density at different charge/discharge rates, a Ragone plot was performed for the supercapacitor unit (Fig. 3f). As the areal power density changed from 100.8 μW cm^{-2} to 500.4 μW cm^{-2}, the areal energy density correspondingly varied from 2.12 μW h cm^{-2} to 1.49 μW h cm^{-2}, which are also remarkable compared to the literature reports.[1–3,38–50] To estimate the cyclic stability of the supercapacitor unit, long-term galvanostatic charge/discharge cycling was performed at a current density of 0.4 mA cm^{-2} (Fig. S3†). After 3000 charge/discharge cycles, the capacitance of supercapacitor unit still showed a retention of ~85%, indicating decent cycling stability. As compared in Table S3,† the performances of the supercapacitor unit of the IPSC in this work were competitive with the existing photo-charging devices.

To investigate the "solar-powering" behaviors of the IPSC, the photo-charging/galvanostatic-discharging mode and photoassisted-galvanostatic-charging/galvanostatic-discharging mode were employed, as detailed in the Experimental section of the ESI.† Fig. 4a shows the photo-charging/galvanostatic-discharging curves of the IPSC. First, the IPSC
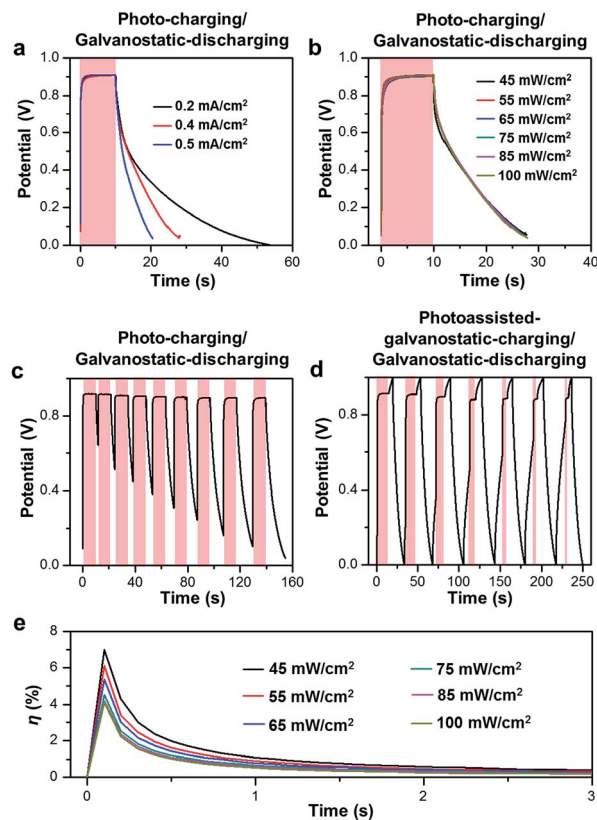
was photo-charged under simulated solar illumination (100 mW cm^{-2}), then the light was turned off and the IPSC was galvanostatic-discharged at different current densities (0.2, 0.4, and 0.5 mA cm^{-2}, respectively). During the charging stage, the photo-charging curves overlapped completely. The voltage of the IPSC rapidly increased to ~0.91 V in less than 1 s under light illumination and then remained stable. During the galvanostatic-discharging stage, the IPSC was discharged from 0.91 V to 0 V within 44, 18, and 11 s at the discharging current densities of 0.2, 0.4, and 0.5 mA cm^{-2}, respectively. The areal capacitances were also calculated, as shown in Fig. S4,† which were in accordance with the results for the galvanostatic-charging/galvanostatic-discharging mode in Fig. 3e. The photo-charging/galvanostatic-discharging behaviors of the IPSC

under different simulated solar illumination intensities (45–100 mW cm^{-2}) were also measured. As shown in Fig. 4b, the time of photo-charging kept very short when the simulated solar illumination intensities decreased from 100 to 45 mW cm^{-2}, suggesting the IPSC can work efficiently at weak light conditions. The partially discharged IPSC could also be fully recharged by photo-charging, as shown in Fig. 4c. The IPSC was first photo-charged to 0.91 V and then partially galvanostatic-discharged to a voltage higher than 0 V; subsequently, the simulated solar illumination (100 mW cm^{-2}) was turned again to recharge the IPSC. It was found that the IPSC could be rapidly re-photo-charged from any partially discharged states to the voltage plateau of 0.91 V.

The working voltage of the IPSC could be further increased to 1.0 V by a photoassisted-galvanostatic-charging/galvanostatic-charging mode. As shown in Fig. 4d, the voltage of the IPSC was first increased close to 0.91 V by galvanostatic-charging (at the current density of 0.4 mA cm^{-2}) coupled with different durations of photo-charging (under the light intensity of 100 mW cm^{-2}), then the light was turned off, and the voltage was further raised to the cutoff voltage of 1.0 V by the still-ongoing galvanostatic-charging. These results confirm that the IPSC can effectively convert solar energy into electric energy by the PSC unit under photo-charging or photoassisted-charging modes, and then stores energy in the supercapacitor unit. The stored electrochemical energy can be released by galvanostatic-discharging, similar to with conventional supercapacitors.

The overall photo-electrochemical energy conversion efficiency (η) of the IPSC was calculated by the following equation:

$$\eta = 0.5C \times V^2/(P_{in} \times S \times t) \tag{1}$$

where C and V are the capacitance and the voltage of the supercapacitor unit, respectively; P_{in} is the power intensity of incident light, S is the effective area of the PSC unit, and t is the photo-charging time. According to the photo-charging/galvanostatic-discharging curves in Fig. 4b, the plots of η versus the photo-charging time (η–t) under different simulated solar illumination intensities (45–100 mW cm^{-2}) are displayed in Fig. 4e. The η–t curves show a volcano shape, which first increases and then decreases during the photo-charging stage. When the power intensity of simulated solar illumination decreased from 100 mW cm^{-2} to 45 mW cm^{-2}, the η reached a peak value of 7.1%, further demonstrating that the IPSC can work efficiently under weak light. Notably, the η obtained from the IPSC is remarkable among the existing integrated photo-powering energy devices (Table S1†).

Conclusions

In summary, by combining a PSC unit and supercapacitor unit into a single device, we developed an integrated solar capacitor with a compact architecture that could simultaneously realize photoelectric energy conversion and electrochemical energy storage. The as-obtained IPSC could perform well under different charging/discharging modes, displaying a high voltage plateau and a high overall energy conversion efficiency, and also

can work efficiently under weak light. We hope this study can provide new insights for the design of integrated energy devices with novel configurations to promote the development of solar utilization and portable power supply technologies.

Conflicts of interest

There are no conflicts to declare.

Acknowledgements

Notes and references

1 J. Liang, G. Zhu, C. Wang, Y. Wang, H. Zhu, Y. Hu, H. Lv, R. Chen, L. Ma, T. Chen, Z. Jin and J. Liu, *Adv. Energy Mater.*, 2017, **7**, 1601208.

2 Z. Yang, J. Deng, H. Sun, J. Ren, S. Pan and H. Peng, *Adv. Mater.*, 2014, **26**, 7038–7042.

3 X. Chen, H. Sun, Z. Yang, G. Guan, Z. Zhang, L. Qiu and H. Peng, *J. Mater. Chem. A*, 2014, **2**, 1897–1902.

4 B. Oregan and M. Gratzel, *Nature*, 1991, **353**, 737–740.

5 A. Yella, H.-W. Lee, H. N. Tsao, C. Yi, A. K. Chandiran, M. K. Nazeeruddin, E. W.-G. Diau, C.-Y. Yeh, S. M. Zakeeruddin and M. Graetzel, *Science*, 2011, **334**, 629–634.

6 D. Irishika, Y. Onitsuka, K. Imamura and H. Kobayashi, *Solar RRL*, 2017, **1**, 1700061.

7 M. Liu, M. B. Johnston and H. J. Snaith, *Nature*, 2013, **501**, 395–398.

8 Y. Lei, X. Yang, L. Gu, H. Jia, S. Ge, P. Xiao, X. Fan and Z. Zheng, *J. Power Sources*, 2015, **280**, 313–319.

9 G. C. Xing, N. Mathews, S. Y. Sun, S. S. Lim, Y. M. Lam, M. Gratzel, S. Mhaisalkar and T. C. Sum, *Science*, 2013, **342**, 344–347.

10 S. D. Stranks, G. E. Eperon, G. Grancini, C. Menelaou, M. J. P. Alcocer, T. Leijtens, L. M. Herz, A. Petrozza and H. J. Snaith, *Science*, 2013, **34234**, 1–344.

11 Y. Hu, S. Si, A. Mei, Y. Rong, H. Liu, X. Li and H. Han, *Solar RRL*, 2017, **1**, 1600019.

12 Q. F. Dong, Y. J. Fang, Y. C. Shao, P. Mulligan, J. Qiu, L. Cao and J. S. Huang, *Science*, 2015, **347**, 967–970.

13 D. W. de Quilettes, S. M. Vorpahl, S. D. Stranks, H. Nagaoka, G. E. Eperon, M. E. Ziffer, H. J. Snaith and D. S. Ginger, *Science*, 2015, **348**, 683–686.

14 J. Burschka, N. Pellet, S. J. Moon, R. Humphry-Baker, P. Gao, M. K. Nazeeruddin and M. Gratzel, *Nature*, 2013, **499**, 316–319.

15 H. P. Zhou, Q. Chen, G. Li, S. Luo, T. B. Song, H. S. Duan, Z. R. Hong, J. B. You, Y. S. Liu and Y. Yang, *Science*, 2014, **345**, 542–546.

16 A. Y. Mei, X. Li, L. F. Liu, Z. L. Ku, T. F. Liu, Y. G. Rong, M. Xu, M. Hu, J. Z. Chen, Y. Yang, M. Gratzel and H. W. Han, *Science*, 2014, **345**, 295–298.

17 M. M. Lee, J. Teuscher, T. Miyasaka, T. N. Murakami and H. J. Snaith, *Science*, 2012, **338**, 643–647.

18 N. J. Jeon, J. H. Noh, W. S. Yang, Y. C. Kim, S. Ryu, J. Seo and S. I. Seok, *Nature*, 2015, **517**, 476–480.

19 H. D. Kim and H. Ohkita, *Solar RRL*, 2017, **1**, 1700027.

20 W. Y. Nie, H. H. Tsai, R. Asadpour, J. C. Blancon, A. J. Neukirch, G. Gupta, J. J. Crochet, M. Chhowalla, S. Tretiak, M. A. Alam, H. L. Wang and A. D. Mohite, *Science*, 2015, **347**, 522–525.

21 D. P. McMeekin, G. Sadoughi, W. Rehman, G. E. Eperon, M. Saliba, M. T. Horantner, A. Haghighirad, N. Sakai, L. Korte, B. Rech, M. B. Johnston, L. M. Herz and H. J. Snaith, *Science*, 2016, **351**, 151–155.

22 W. Chen, Y. Z. Wu, Y. F. Yue, J. Liu, W. J. Zhang, X. D. Yang, H. Chen, E. B. Bi, I. Ashraful, M. Gratzel and L. Y. Han, *Science*, 2015, **350**, 944–948.

23 X. Li, D. Q. Bi, C. Y. Yi, J. D. Decoppet, J. S. Luo, S. M. Zakeeruddin, A. Hagfeldt and M. Gratzel, *Science*, 2016, **353**, 58–62.

24 L. T. Dou, A. B. Wong, Y. Yu, M. L. Lai, N. Kornienko, S. W. Eaton, A. Fu, C. G. Bischak, J. Ma, T. N. Ding, N. S. Ginsberg, L. W. Wang, A. P. Alivisatos and P. D. Yang, *Science*, 2015, **349**, 1518–1521.

25 W. S. Yang, B.-W. Park, E. H. Jung, N. J. Jeon, Y. C. Kim, D. U. Lee, S. S. Shin, J. Seo, E. K. Kim, J. H. Noh and S. I. Seok, *Science*, 2017, **356**, 1376–1379.

26 J. Liang, C. Wang, Y. Wang, Z. Xu, Z. Lu, Y. Ma, H. Zhu, Y. Hu, C. Xiao, X. Yi, G. Zhu, H. Lv, L. Ma, T. Chen, Z. Tie, Z. Jin and J. Liu, *J. Am. Chem. Soc.*, 2016, **138**, 15829–15832.

27 J. Liang, C. Wang, Y. Wang, Z. Xu, Z. Lu, Y. Ma, H. Zhu, Y. Hu, C. Xiao, X. Yi, G. Zhu, H. Lv, L. Ma, T. Chen, Z. Tie, Z. Jin and J. Liu, *J. Am. Chem. Soc.*, 2017, **139**, 2852.

28 Z. Ku, Y. Rong, M. Xu, T. Liu and H. Han, *Sci. Rep.*, 2013, **3**, 3132.

29 X. Xu, Z. Liu, Z. Zuo, M. Zhang, Z. Zhao, Y. Shen, H. Zhou, Q. Chen, Y. Yang and M. Wang, *Nano Lett.*, 2015, **15**, 2402–2408.

30 H. Wei, J. Xiao, Y. Yang, S. Lv, J. Shi, X. Xu, J. Dong, Y. Luo, D. Li and Q. Meng, *Carbon*, 2015, **93**, 861–868.

31 H. Chen, Z. Wei, H. He, X. Zheng, K. S. Wong and S. Yang, *Adv. Energy Mater.*, 2016, **6**, 1502087.

32 Z. Liu, B. Sun, T. Shi, Z. Tang and G. Liao, *J. Mater. Chem. A*, 2016, **4**, 10700–10709.

33 X. Li, M. Tschumi, H. Han, S. S. Babkair, R. A. Alzubaydi, A. A. Ansari, S. S. Habib, M. K. Nazeeruddin, S. M. Zakeeruddin and M. Graetzel, *Energy Technol.*, 2015, **3**, 551–555.

34 Z. Yang, L. Li, Y. Luo, R. He, L. Qiu, H. Lin and H. Peng, *J. Mater. Chem. A*, 2013, **1**, 954–958.

35 N. F. Yan, G. R. Li, G. L. Pan and X. P. Gao, *J. Electrochem. Soc.*, 2012, **159**, A1770–A1774.

36 P. Liu, H. X. Yang, X. P. Ai, G. R. Li and X. P. Gao, *Electrochem. Commun.*, 2012, **16**, 69–72.

37 P. Liu, Y.-L. Cao, G.-R. Li, X.-P. Gao, X.-P. Ai and H.-X. Yang, *ChemSusChem*, 2013, **6**, 802–806.

38 J. Xu, H. Wu, L. Lu, S.-F. Leung, D. Chen, X. Chen, Z. Fan, G. Shen and D. Li, *Adv. Funct. Mater.*, 2014, **24**, 1840–1846.

39 Y. Fu, H. Wu, S. Ye, X. Cai, X. Yu, S. Hou, H. Kafafy and D. Zou, *Energy Environ. Sci.*, 2013, **6**, 805–812.

40 A. P. Cohn, W. R. Erwin, K. Share, L. Oakes, A. S. Westover, R. E. Carter, R. Bardhan and C. L. Pint, *Nano Lett.*, 2015, **15**, 2727–2731.

41 M. Yu, W. D. McCulloch, D. R. Beauchamp, Z. Huang, X. Ren and Y. Wu, *J. Am. Chem. Soc.*, 2015, **137**, 8332–8335.

42 Y. Sun and X. Yan, *Solar RRL*, 2017, **1**, 1700002.

43 X. Xu, S. Li, H. Zhang, Y. Shen, S. M. Zakeeruddin, M. Graetzel, Y.-B. Cheng and M. Wang, *ACS Nano*, 2015, **9**, 1782–1787.

44 P. Du, X. Hu, C. Yi, H. C. Liu, P. Liu, H.-L. Zhang and X. Gong, *Adv. Funct. Mater.*, 2015, **25**, 2420–2427.

45 J. T. Xu, Y. H. Chen and L. M. Dai, *Nat. Commun.*, 2015, **6**, 8103.

46 J. Xu, Z. Ku, Y. Zhang, D. Chao and H. J. Fan, *Adv. Mater. Technol.*, 2016, **1**, 1600074.

47 S. C. Liao, X. Zong, B. Seger, T. Pedersen, T. T. Yao, C. M. Ding, J. Y. Shi, J. Chen and C. Li, *Nat. Commun.*, 2016, **7**, 11474.

48 M. Z. Yu, X. D. Ren, L. Ma and Y. Y. Wu, *Nat. Commun.*, 2014, **5**, 5111.

49 T. Chen, L. B. Qiu, Z. B. Yang, Z. B. Cai, J. Ren, H. P. Li, H. J. Lin, X. M. Sun and H. S. Peng, *Angew. Chem., Int. Ed.*, 2012, **51**, 11977–11980.

50 Z. T. Zhang, X. L. Chen, P. N. Chen, G. Z. Guan, L. B. Qiu, H. J. Lin, Z. B. Yang, W. Y. Bai, Y. F. Luo and H. S. Peng, *Adv. Mater.*, 2014, **26**, 466–470.

51 D. Pech, M. Brunet, H. Durou, P. Huang, V. Mochalin, Y. Gogotsi, P.-L. Taberna and P. Simon, *Nat. Nanotechnol.*, 2010, **5**, 651–654.

52 Y. Zhu, S. Murali, M. D. Stoller, K. J. Ganesh, W. Cai, P. J. Ferreira, A. Pirkle, R. M. Wallace, K. A. Cychosz, M. Thommes, D. Su, E. A. Stach and R. S. Ruoff, *Science*, 2011, **332**, 1537–1541.

53 J. A. Lee, M. K. Shin, S. H. Kim, H. U. Cho, G. M. Spinks, G. G. Wallace, M. D. Lima, X. Lepro, M. E. Kozlov, R. H. Baughman and S. J. Kim, *Nat. Commun.*, 2013, **4**, 1970.

54 Z. Yang, J. Deng, X. Chen, J. Ren and H. Peng, *Angew. Chem., Int. Ed.*, 2013, **52**, 13453–13457.

55 D. Yu, K. Goh, H. Wang, L. Wei, W. Jiang, Q. Zhang, L. Dai and Y. Chen, *Nat. Nanotechnol.*, 2014, **9**, 555–562.

56 T. Kim, G. Jung, S. Yoo, K. S. Suh and R. S. Ruoff, *ACS Nano*, 2013, **7**, 6899–6905.

57 Z. Tang, C.-H. Tang and H. Gong, *Adv. Funct. Mater.*, 2012, **22**, 1272–1278.

58 L. L. Zhang and X. S. Zhao, *Chem. Soc. Rev.*, 2009, **38**, 2520–2531.

59 B. Liu, B. Liu, X. Wang, X. Wu, W. Zhao, Z. Xu, D. Chen and G. Shen, *Adv. Mater.*, 2014, **26**, 4999–5004.

60 X. Wang, B. Liu, R. Liu, Q. Wang, X. Hou, D. Chen, R. Wang and G. Shen, *Angew. Chem., Int. Ed.*, 2014, **53**, 1849–1853.

61 J. Li, J. Yao, H. Xia, W. Sun, J. Liu and L. Peng, *Appl. Phys. Lett.*, 2014, **24**, 1840.